Hyperfine splittings of neonlike lasing lines

James H. Scofield and Joseph Nilsen
Lawrence Livermore National Laboratory, Livermore, California 94550
(Received 14 October 1993)

The hyperfine splitting of a soft-x-ray lasing line coming from neonlike niobium has recently been measured and the effect of the splitting on the gain coefficient observed, as reported earlier. In this work, the hyperfine splittings for the principal $3p \rightarrow 3s$ neonlike lasing lines due to the coupling with the dipole magnetic moment of the nucleus are calculated for atomic numbers Z from 17 through 59 in the framework of the relativistic multiconfiguration-atomic-structure theory. The diminution of the gains due to the splittings in the case of Doppler-broadened lines is calculated. The parameters for the splitting of the $2p$-to-$2s$ transitions in fluorinelike ions and the $3p$-to-$3s$ and $3d$-to-$3p$ transitions in sodiumlike ions are also presented.

PACS number(s): 31.30.Gs, 32.70.Jz, 42.55.Vc

INTRODUCTION

Recently, the hyperfine splittings of a Ne-like lasing line of niobium within a plasma heated by an optical laser has been observed and the effect of the splittings has served as a possible explanation of observed low laser emissions of Ne-like ions for elements with odd atomic numbers Z [1]. This paper reports the results of calculations of the hyperfine line splittings and their effect on the gain coefficient for the $3p \rightarrow 3s$ Ne-like lasing lines. Hyperfine splittings of neutral and near-neutral ions have long been observed and understood [2]. Perturbed angular correlations from the hyperfine coupling in decays of stripped low-Z ions have been routinely used to obtain the nuclear moments [3]. Several recent studies have looked at the effects of the hyperfine coupling in highly stripped ions. These have included the effect on polarization of radiation from He-like lines [4] and on the emission rates of such emission [5]. Hyperfine splittings of lines of kryptonlike niobium have been observed [6]. The transition between the hyperfine-split levels of the $1s$ state of hydrogenlike bismuth has been recently observed in a fluorescence experiment [7].

The question of the hyperfine splittings was examined for the Ne-like lasing lines after lasing was observed for the even Z elements ($Z=22$, 24, and 26) but was not observed in the odd-Z elements ($Z=21$ and 23) [8–11]. Recent comparison between the lasing transitions in Ne-like Nb ($Z=41$) and Zr ($Z=40$) observed a dramatic change in the ratio of the standard $J=2\rightarrow 1$ and the $0\rightarrow 1$ lines [12]. The width of the laser lines determine their strengths at the center of the line and are therefore an important factor in determining their gain coefficient. The hyperfine splittings will increase the width beyond that of the normal thermal Doppler broadening of the lines. If the hyperfine splittings are large enough, a single line is split into a set of lines with diminished line strengths. This split was observed in the case of niobium which has a large nuclear magnetic moment for a Z small enough to make lasing experimentally achievable.

The lasing on the $3p \rightarrow 3s$ lines in the Ne-like ions comes about by populating of the $3p$ levels by electron collisional excitations from the ground states as well as transitions from other Ne-, F-, and Na-like states [13]. An inversion can exist between the $3p$ states and the $3s(J=1)$ states due to the slow decay of the $3p$ states in comparison with the $3s$ states which rapidly radiatively decay to the $2p^6$ ground state. There are two $3s(J=1)$ states. For the higher Z's, for which jj coupling is appropriate, these correspond to the $2p$ vacancy in either the $2p_{3/2}$ or $2p_{1/2}$ states. These states go over to the $^3P_1$ or $^1P_1$ configurations, respectively, for low Z's. The hyperfine splittings for the $2p_{1/2}$ vacancy states are larger than those for the $2p_{3/2}$ states. The electron's spin and orbital angular momenta contribute with opposite sign to the splittings and thus add together in the $2p_{1/2}$ case and subtract in the $2p_{3/2}$ case. The $2p_{1/2}$ state also has increased splittings at high Z's due to relativistic corrections. In addition, for the $2p_{3/2}3s_{1/2}(J=1)$ state, there is a large cancellation between the contributions from the $2p$ and $3s$ electron.

In Table I a key is given for the five Ne-like lines calculated to have the strongest gain coefficient in the mid-Z region. Vacancies in the Ne-like core are denoted by an overbar. For these lines the vacancy state is preserved in the transition. In the low-Z region, line E, originating from the $\overline{2p_{1/2}}3p_{1/2}(J=0)$ level is strongest. At higher Z's, lines A and B originating with the $\overline{2p_{3/2}}3p_{3/2}(J=2)$ and $\overline{2p_{1/2}}3p_{3/2}(J=2)$ levels are the strongest. The lines, C and D, originating with the $\overline{2p_{3/2}}3p_{1/2}(J=2)$ and the $\overline{2p_{3/2}}3p_{3/2}(J=1)$ levels are also prominent. Four additional lines have been seen to weakly lase. The two $3p$-to-$3s$ transitions, $\overline{2p_{3/2}}3p_{3/2}(J=0)\rightarrow\overline{2p_{3/2}}3s_{1/2}(J=1)$ and $\overline{2p_{1/2}}3p_{1/2}(J=0)\rightarrow\overline{2p_{3/2}}3s_{1/2}(J=1)$, have very small hyperfine splittings. The first line has been observed at higher Z [12,14,15] and the second at lower Z [9,10,16]. The two $2s$ vacancy transitions, $\overline{2s_{1/2}}3d_{3/2}(J=2)\rightarrow\overline{2s_{1/2}}3p_{1/2}(J=1)$ and $\overline{2s_{1/2}}3d_{5/2}(J=2)\rightarrow\overline{2s_{1/2}}3p_{3/2}(J=1)$, have hyperfine splittings as large as those reported here but the lines have been seen very infrequently [16,17]. These four lines are not treated further here.

TABLE I. Key used for the naming of the neonlike lasing lines.

Key	Upper	J	Lower	J	$\gamma(Z=41)$ (Å)
A	$\overline{2p}_{3/2}3p_{3/2}$	2	$\overline{2p}_{3/2}3s_{1/2}$	1	138.6
B	$\overline{2p}_{1/2}3p_{3/2}$	2	$\overline{2p}_{1/2}3s_{1/2}$	1	140.4
C	$\overline{2p}_{3/2}3p_{1/2}$	2	$\overline{2p}_{3/2}3s_{1/2}$	1	202.5
D	$\overline{2p}_{3/2}3p_{3/2}$	1	$\overline{2p}_{3/2}3s_{1/2}$	1	147.6
E	$2p_{1/2}3p_{1/2}$	0	$2p_{1/2}3s_{1/2}$	1	145.9

HYPERFINE ENERGY SPLITTING OF NEONLIKE IONS

The major contribution to the hyperfine splitting is the interaction of the magnetic field of the nucleus due to its magnetic-dipole moment with the orbital electrons. There is an additional contribution from the electric quadrupole moment of the nucleus but this is quite small in the cases considered in this paper.

For the magnetic-dipole hyperfine interaction, the vector field, $\mathbf{A}$, of the nucleus [18–20],

$$\mathbf{A}(r)=\boldsymbol{\mu}\times\frac{\hat{\mathbf{r}}}{r^2}=\frac{\mu}{I}\mathbf{I}\times\frac{\hat{\mathbf{r}}}{r^2}\ , \tag{1}$$

with μ the magnetic moment of the nucleus and I its spin, interacts with the atomic electrons with the interaction

$$H_{\rm hyp}=e\sum_k \boldsymbol{\alpha}_k\cdot\mathbf{A}(r_k)=\left[\frac{e\mu}{I}\right]\sum_k \mathbf{I}\cdot\frac{\hat{\mathbf{r}}_k}{r_k^2}\times\boldsymbol{\alpha}_k=\left[\frac{e\mu}{I}\right]\sum_{k,q}(-1)^q I^{(1)}_{-q}h^{(1)}_{kq}\ , \tag{2}$$

$$h^{(1)}_{kq}=\frac{-i\boldsymbol{\alpha}_k\cdot\mathbf{L}_k C^{(1)}_q(\hat{\mathbf{r}}_k)}{r_k^2}\ , \tag{3}$$

where $\boldsymbol{\alpha}$ denotes the Dirac matrices, k the individual electrons, and q the spherical tensor components, and

$$C^{(1)}_q(\hat{\mathbf{r}}_k)=\left[\frac{4\pi}{3}\right]^{1/2}Y_{1q}(\hat{\mathbf{r}}_k)\ , \tag{4}$$

$$\mathbf{L}=-i\mathbf{r}\times\nabla\ . \tag{5}$$

The coupling of an atomic state with angular momentum J and the nucleus with spin I gives a total angular momentum F. The matrix element of the total wave function,

$$\Psi_{FM}=\sum(-1)^{I-J+M}(2F+1)^{1/2}\begin{pmatrix}F & I & J\\ -M & \mu & \nu\end{pmatrix}\chi_{I\mu}\psi_{J\nu}\ , \tag{6}$$

is given by

$$(\gamma' IJ'FM|H_{\rm hyp}|\gamma IJFM)=\left[\frac{e\mu}{I}\right](-1)^{I+J'+F}\begin{Bmatrix}F & J' & I\\ 1 & I & J\end{Bmatrix}\times\langle I\|I\|I\rangle\left\langle\gamma'J'\left|\left|\sum_k h^{(1)}_k\right|\right|\gamma J\right\rangle\ . \tag{7}$$

The magnetic subshell dependence has been taken out with the introduction of the reduced matrix elements defined by

$$(j_1m_1|T^k_q|j_2m_2)=(-1)^{j_1-m_1}\begin{pmatrix}j_1 & k & j_2\\ -m_1 & q & m_2\end{pmatrix}\langle j_1\|T^k\|j_2\rangle\ , \tag{8}$$

for a generic operator T. We have explicit values

$$\begin{Bmatrix}F & J & I\\ 1 & I & J\end{Bmatrix}=(-1)^{F+I+J+1}\times\frac{[I(I+1)+J(J+1)-F(F+1)]}{2[I(I+1)(2I+1)J(J+1)(2J+1)]^{1/2}} \tag{9}$$

and

$$\langle I||I||I\rangle=[I(I+1)(2I+1)]^{1/2} \tag{10}$$

for the angular-momentum operator I.

If the atomic states are not coupled, we can effectively put

$$H_{\rm hyp}=\frac{\mu}{\mu_N I}A_e\mathbf{I}\cdot\mathbf{J} \tag{11}$$

with

$$A_e=e\mu_N\left\langle\gamma J\left|\left|\sum_k h^{(1)}_k\right|\right|\gamma J\right\rangle\Big/\langle J\|J\|J\rangle \tag{12}$$

and

$$\mu_N=\frac{e\hbar}{2M_pc}=2.002\times10^{-6}\ \text{(a.u.)}\ . \tag{13}$$

The quantity A_e depends only on the atomic properties and thus has a systematic variation in going from element to element. The energy shift due to the hyperfine interaction is

$$\langle F\|H_{\rm hyp}\|F\rangle=\frac{\mu}{\mu_N I}\frac{A_e}{2}[F(F+1)-I(I+1)-J(J+1)]\ , \tag{14}$$

where F can range from $|I-J|$ to $(I+J)$ and the energy spread across the complex is given by

$$\Delta E=\frac{\mu}{\mu_N I}A_e\times\begin{cases}J(2I+1)\ , & I\geq J\\ I(2J+1)\ , & I\leq J\ .\end{cases} \tag{15}$$

The calculations reported here have been carried out by using a slightly modified version of the relativistic multiconfiguration Hartree-Fock GRASP computer code [21]. The mixing of the states with an electron excited

from the $n=2$ core to the $n=3$ shell were included. For the elements away from the low end of the Periodic Table, the states are quite pure in jj coupling and the matrix elements follow easily from the single-particle matrix elements. The matrix elements are a sum of an angular factor times a single-particle matrix element for each open shell. For the $h^{(1)}$ operator here with the $k=1$ odd rank, the matrix elements between the single vacancy states are identical to those between two single-particle states.

With only the one configuration included, the explicit expression giving the matrix element for the coupled states in terms of the single-particle matrix elements is

$$\langle (j_1 j_2)J \| h \| (j_1 j_2)J \rangle = C(j_1,j_2,J)\langle j_1 \| h \| j_1 \rangle + C(j_2,j_1,J)\langle j_2 \| h \| j_2 \rangle , \quad (16)$$

with

$$C(j_1,j_2,J)=(-1)^{(J+j_1+j_2+1)} \times (2J+1) \begin{Bmatrix} 1 & J & J \\ j_2 & j_1 & j_1 \end{Bmatrix} . \quad (17)$$

The single-particle matrix elements are here given by

$$\langle j \| h \| j \rangle = (-1)^{j-1/2}(2j+1) \begin{bmatrix} j & 1 & j \\ \frac{1}{2} & 0 & -\frac{1}{2} \end{bmatrix} \times 4\kappa \int \frac{p(r)q(r)}{r^2} dr , \quad (18)$$

in which

$$\begin{bmatrix} j & 1 & j \\ \frac{1}{2} & 0 & -\frac{1}{2} \end{bmatrix} = \frac{(-1)^{j-1/2}}{2[(2j+1)(j+1)j]^{1/2}} \quad (19)$$

and p and q are the large and small component radial wave functions and κ is the relativistic angular quantum number,

$$|\kappa| = j + \tfrac{1}{2} .$$

Nonrelativistically we have

$$\kappa \int \frac{p(r)q(r)}{r^2} dr = \frac{Z^3\alpha}{(2l+1)n^3} \quad (20)$$

for a pure Coulomb potential, or with the terms collected for the Coulomb expression

$$\langle j \| h \| j \rangle = \frac{2Z^3\alpha(2j+1)^{1/2}}{(2l+1)n^3[j(j+1)]^{1/2}} R(j) . \quad (21)$$

A relativistic correction, which is quite accurate for hydrogenlike ions and given originally by Racah [22], has been introduced.

$$R(j) = \frac{2j(j+1)(2j+1)}{\gamma(4\gamma^2-1)} , \quad (22)$$

with

$$\gamma = \sqrt{\kappa^2-(Z\alpha)^2} . \quad (23)$$

Table II presents the single-particle matrix elements and their coefficients for the various states, leading to the matrix elements in the case of niobium. The state matrix elements include the contributions from the other configurations. Equation (21) has been worked backwards to give the effective Z's in the table. The large cancellation between the $2p_{3/2}$ and $3s$ contributions to the $\overline{2p_{3/2}3s_{1/2}}(J=1)$ lower lasing state is seen.

The finite nuclear size is here taken into account as far as the electronic wave functions are concerned. It has not been taken into account in the source of the magnetic field of the nucleus. That is, we have omitted the so called Bohr-Weisskopf effect [23]. Even for high-Z elements, the correction is at most of the order of a couple of percent.

Table III presents the A_e for the odd-Z elements ranging from $Z=17$ through $Z=59$. Figure 1 plots A_e for the various states. In general, due to the screening effects, the curves show a dependence closer to Z^4 than to the Z^3 dependence for the hydrogenic ions. The exceptions are for the $\overline{2p_{1/2}3s_{1/2}}(J=1)$ state in which there are level crossings around $Z=51$ and 55, the $\overline{2p_{3/2}3s_{1/2}}(J=1)$ state for which the $2p$ and $3s$ contributions cancel, and the $\overline{2p_{3/2}3p_{3/2}}(J=1)$ which is mixed

TABLE II. Composition of the matrix element for the states, $\langle \gamma J \| h \| \gamma J \rangle$ in a.u., as the sum of the coefficients $C(j_1,j_2,J)$ times the single-particle matrix elements for the levels of neonlike niobium. The total includes contributions from the other configurations.

Quantity \ nl_{j_1}	$2p_{1/2}$	$2p_{3/2}$	$3s_{1/2}$	$3p_{1/2}$	$3p_{3/2}$
effective Z	37.83	37.61	36.55	35.78	35.63
$\langle nl_{j_1} \| h \| nl_{j_1} \rangle$	63.87	34.54	51.38	16.04	8.738

State	J	Coefficient $C(j_1,j_2,J)$					$\langle \gamma J \| h \| \gamma J \rangle$	A_e (meV)
$\overline{2p_{1/2}3s_{1/2}}$	1	1.0		1.0			115.0	2.55
$\overline{2p_{1/2}3p_{3/2}}$	2	1.118				1.061	80.57	0.800
$\overline{2p_{3/2}3s_{1/2}}$	1		0.7906	−0.5			1.576	0.038
$\overline{2p_{3/2}3p_{3/2}}$	2		0.7071			0.7071	30.59	0.304
$\overline{2p_{3/2}3p_{1/2}}$	2		1.061		1.118		54.44	0.542
$\overline{2p_{3/2}3p_{3/2}}$	1		0.3162			0.3162	14.72	0.328

TABLE III. Values of the coefficients A_e given in meV for the various levels with the total J given in parentheses.

Z	$\overline{2p}_{1/2}3s_{1/2}$ (1)	$\overline{2p}_{1/2}3p_{3/2}$ (2)	$\overline{2p}_{3/2}3s_{1/2}$ (1)	$\overline{2p}_{3/2}3p_{3/2}$ (2)	$\overline{2p}_{3/2}3p_{1/2}$ (2)	$\overline{2p}_{3/2}3p_{3/2}$ (1)
71	0.081	0.030	0.024	0.014	0.022	0.009
19	0.135	0.048	0.026	0.021	0.034	0.045
21	0.207	0.070	0.027	0.030	0.050	0.055
23	0.298	0.099	0.029	0.042	0.069	0.067
25	0.412	0.134	0.032	0.056	0.095	0.083
27	0.550	0.178	0.035	0.073	0.125	0.101
29	0.717	0.230	0.038	0.094	0.161	0.122
31	0.917	0.293	0.042	0.118	0.204	0.146
33	1.152	0.366	0.044	0.146	0.254	0.173
35	1.429	0.452	0.046	0.178	0.312	0.204
37	1.751	0.552	0.046	0.215	0.379	0.240
39	2.124	0.668	0.044	0.257	0.455	0.281
41	2.554	0.800	0.038	0.304	0.542	0.328
43	3.046	0.952	0.028	0.356	0.639	0.380
45	3.606	1.124	0.014	0.415	0.749	0.438
47	4.239	1.320	−0.007	0.479	0.872	0.503
49	4.930	1.542	−0.036	0.551	1.010	0.574
51	4.960	1.793	−0.075	0.629	1.163	0.652
53	6.310	2.077	−0.125	0.714	1.333	0.738
55	4.805	2.396	−0.189	0.807	1.521	0.831
57	8.727	2.756	−0.270	0.909	1.731	0.933
59	10.324	3.161	−0.371	1.019	1.961	1.043

strongly with the $\overline{2p}_{3/2}3p_{1/2}(J=1)$ state for Z's below 35.

TRANSITIONS

For uncoupled atomic states, the transition rate to go from one hyperfine state to a second ($F \rightarrow F'$) is given by

$$\Gamma_{FF'} = (2F'+1)(2J+1) \begin{Bmatrix} F' & J' & I \\ J & F & 1 \end{Bmatrix}^2 \Gamma_{JJ'} \tag{24}$$

for $E1$ transitions in which $\Gamma_{JJ'}$ is the rate of decay for the atomic state. We make the assumption here that the hyperfine components of the upper state are statistically populated. These rates coupled with the line splittings and the broadening give the emission spectra.

For the nuclear spin values $I > \frac{1}{2}$, the $J=1$ states are split into three components which results in the $J=0 \rightarrow 1$ lines being split into three components and the $J=1 \rightarrow 1$ lines split into seven components. For $I > \frac{3}{2}$ the $J=2 \rightarrow 1$ transitions are split into nine components. These components will be merged together if the natural widths are large enough. Figure 2 shows the example of the relative gain of the $\overline{2p}_{1/2}3p_{1/2}(J=0)$ to $\overline{2p}_{1/2}3s_{1/2}(J=1)$ transition in niobium due to a Doppler-broadened line with a 600-eV ion temperature. The gain is normalized to unity for the case of no hyperfine splitting. The dotted lines

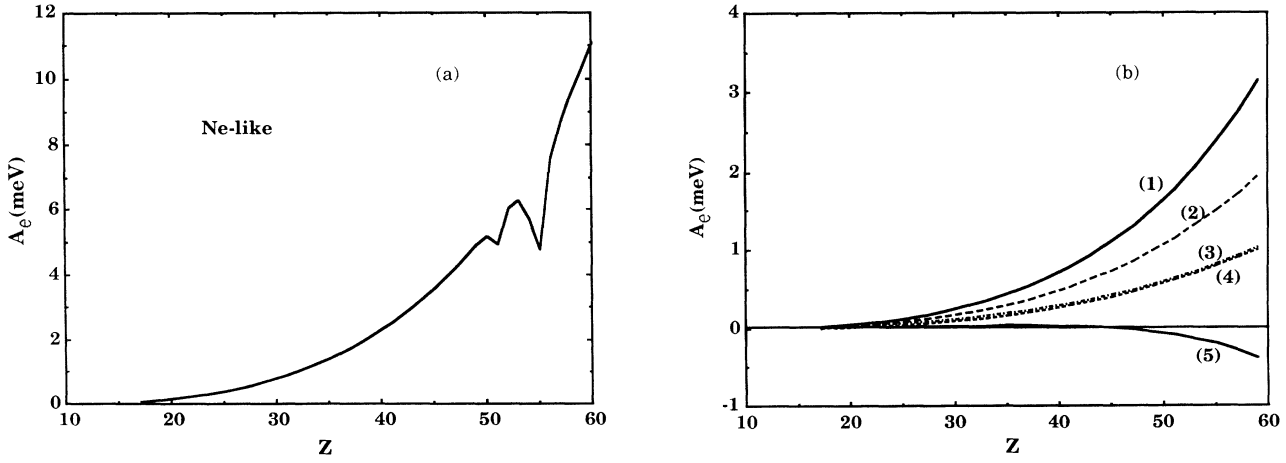

FIG. 1. (a) The coefficient A_e vs Z for the $\overline{2p}_{1/2}3s_{1/2}(J=1)$ level. (b) The coefficient A_e vs Z. The curves are labeled by (1) $\overline{2p}_{1/2}3p_{3/2}(J=2)$, (2) $\overline{2p}_{3/2}3p_{1/2}(J=2)$, (3) $\overline{2p}_{3/2}3p_{3/2}(J=1)$, (4) $\overline{2p}_{3/2}3p_{3/2}(J=2)$, and (5) $\overline{2p}_{3/2}3s_{1/2}(J=1)$.

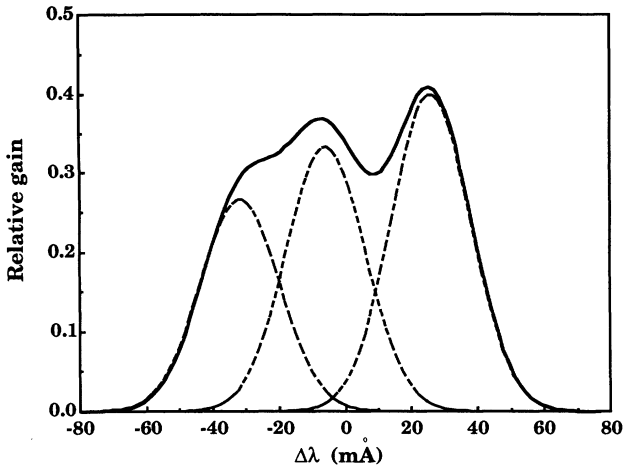

FIG. 2. Relative gain coefficients as a function of wavelength due to the hyperfine splitting of line E in niobium for an ion temperature of 600 eV. The dashed lines show the contributions due to each of the components. The gain is normalized to unity for no hyperfine splitting.

show the individual components while the solid line gives the sum. The line is split into two distinct components with the third component blended. For the $2p_{1/2}3p_{3/2}(J=2)$ to $2p_{1/2}3s_{1/2}(J=1)$ transition, shown in Fig. 3, the nine components all blend together to make a single line with a 60% broader width than without the hyperfine effect. Table IV presents the nuclear parameters [24] used and the total separation of the outer most of the complex of lines. Even though the $J=2$ to 1, line B, has, in general, more components than the $J=0$ to 1, line E, they have the same total splitting since they share the same lower laser state and that dominates the splitting. With three hyperfine components to line E, the two stronger components are split apart by $(I+1)/(2I+1)$ of the total splitting. Calculationally these two components in niobium are split by 19.3 meV or 33 mÅ. This is in good agreement with the observed splittings between the peaks of 28 mÅ [1].

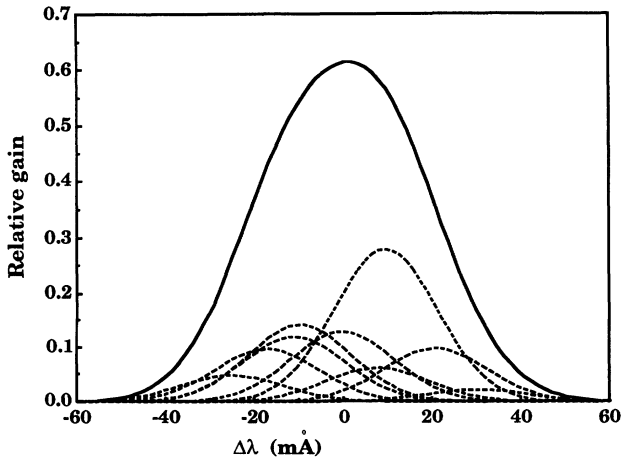

FIG. 3. Relative gain coefficient due to hyperfine splitting of line B in niobium for an ion temperature of 600 eV.

LINE BROADENING AND GAINS

If the hyperfine splittings are to have an effect on the laser emission, their splittings must not be much smaller than the other broadenings. Under most conditions the major broadening is the Doppler broadening due to the ion motion.

This gives a distribution in photon energy from the center of the line

$$I(\varepsilon)=\frac{1}{\sqrt{2\pi}D}\exp\left[-\frac{1}{2}\left[\frac{\varepsilon}{D}\right]^2\right], \tag{25}$$

with

$$D=E_0(kT/Mc^2)^{1/2} \tag{26}$$

and

$$\varepsilon=E-E_0\ , \tag{27}$$

the displacement of the photon energy, E, from line center, E_0. kT is the ion temperature, D the rms width of

TABLE IV. Nuclear parameters and the split across the transition arrays in meV for the various transitions. AM is the atomic mass.

Z	AM	I	μ	A	B,E	C	D
17	35	$\frac{3}{2}$	0.822	0.053	0.174	0.074	0.053
17	37	$\frac{3}{2}$	0.684	0.044	0.145	0.062	0.044
19	39	$\frac{3}{2}$	0.391	0.033	0.142	0.053	0.048
21	45	$\frac{7}{2}$	4.756	0.413	2.25	0.784	0.596
23	51	$\frac{7}{2}$	5.151	0.636	3.51	1.27	0.793
25	55	$\frac{5}{2}$	3.453	0.679	3.42	1.32	0.697
27	59	$\frac{7}{2}$	4.628	1.170	5.82	2.29	1.08
29	63	$\frac{3}{2}$	2.223	0.872	4.24	1.58	0.721
29	65	$\frac{3}{2}$	2.382	0.938	4.55	1.70	0.772
31	69	$\frac{3}{2}$	2.017	1.080	4.94	1.98	0.781
33	75	$\frac{3}{2}$	1.439	1.013	4.43	1.86	0.652
35	79	$\frac{3}{2}$	2.106	1.80	8.04	3.30	1.13
35	81	$\frac{3}{2}$	2.271	1.93	8.66	3.53	1.22
37	85	$\frac{5}{2}$	1.353	1.22	5.69	2.35	0.766
37	87	$\frac{3}{2}$	2.751	2.80	12.9	5.10	1.75
39	89	$\frac{1}{2}$	−0.137	0.177	0.876	0.313	0.134
41	93	$\frac{9}{2}$	6.171	7.85	35.0	14.3	4.51
43	99	$\frac{9}{2}$	5.685	8.61	38.5	15.8	4.78
45	103	$\frac{1}{2}$	−0.088	0.183	0.956	0.331	0.120
47	107	$\frac{1}{2}$	−0.114	0.275	1.44	0.498	0.174
47	109	$\frac{1}{2}$	0.131	0.316	1.66	0.572	0.200
49	115	$\frac{9}{2}$	5.541	13.9	60.7	25.5	7.86
51	121	$\frac{5}{2}$	3.363	10.8	40.0	19.3	5.99
51	123	$\frac{7}{2}$	2.55	7.83	28.9	13.9	4.34
53	127	$\frac{5}{2}$	2.813	10.8	42.6	18.4	6.76
55	133	$\frac{7}{2}$	2.582	10.6	28.4	19.1	6.02
57	139	$\frac{7}{2}$	2.783	13.2	55.5	23.8	7.52
59	141	$\frac{5}{2}$	4.136	23.9	102.5	42.6	14.1

the distribution, and M the ion mass. We here parameterized the hyperfine splittings in terms of a temperature, kT_0:

$$kT_0 = \left[\frac{\Delta E_{\rm rms}}{E}\right]^2 Mc^2 , \tag{28}$$

in which here $\Delta E_{\rm rms}$ is the rms splitting due to the hyperfine splittings. Table V lists the kT_0 for the odd elements. For small values of kT/kT_0 the drop in the peak emission strength and thus in the gain coefficient is a universal function. This holds fairly well down to the point that the individual peaks are being separated. Figure 4 shows the peak relative gain coefficient as a function of T/T_0 for the transitions in niobium and for transition E in vanadium.

The question now is as to the actual ion temperatures in the lasers. To work, the collisionally excited lasers require a bath of high-temperature electrons to ionize and excite the ions. On the other hand, low ion temperatures lead to higher gain coefficients due to the narrowing of the lines. There is a paucity of experimental information on the conditions existing in the plasmas at the time of lasing. Theoretical studies show an electron temperature of roughly

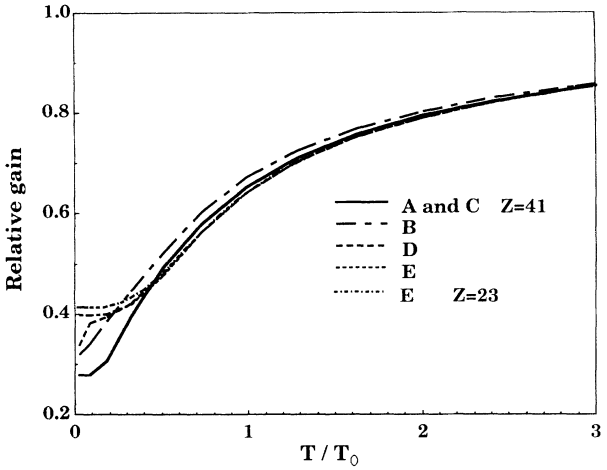

FIG. 4. Relative peak gain coefficient due to the hyperfine splitting as a function of the ion temperature divided by the temperature corresponding to the rms splitting of the lines for the lines in niobium and line E in vanadium.

$$kT_e = 1700\left[\frac{Z}{41}\right]^{7/2} \text{eV} \tag{29}$$

is required to produce the neonlike ions with enough excitation for lasing [25,26]. The ions are heated in collisions by the electrons and they lose energy in expanding the material. Simulation studies show a variation in the expected ion temperature depending on the details of the plasma. To assess the importance of the hyperfine splittings, ion temperatures were obtained from simulations using the LASNEX hydrodynamic code [27] to model both the blow off from a solid slab target heated by a single beam and the heating of a foil heated from both sides. The beams were chosen to be a full width half maximum pulse of 600 ps with a strength to produce the neonlike stage. The lower ion temperatures were obtained for the slab targets for Z's below 34 and for the foil for Z's above 34. Table VI gives these ion temperatures and the relative gain coefficient due to the hyperfine splittings for transitions B, C, and E, which suffer the largest effect due to the hyperfine splittings. The ion temperatures used here range between one-fifth and one-third of the nominal electron temperature. They can be compared to calculated values given in the literature for T_I of 50 eV at $Z=22$ [9], 400 eV at $Z=34$ [28], and 700 eV at $Z=41$ [1] vs 53, 324, and 600 eV corresponding to the values used here. The one measurement of the actual laser line width can be interpreted as being due to a higher temperature than the theoretical value for $Z=34$ [29].

Figure 5 plots for lines B, C, and E the ion temperature for which the gain coefficient is dropped to 70% of its standard value along with the nominal temperature for lasing. If the ion temperature is below that plotted for a transition, the gain will drop by more than 30% due to the hyperfine splitting. For Z's of 39, 45, and 47 the hyperfine splitting is so small that ion temperatures below 10 eV would be needed before they would cause a 30% drop in gain.

TABLE V. The rms spread of the transition arrays for lines A to E given in terms of the temperature parameter, kT_0, in eV for Ne-like ions with nuclear charge Z and atomic mass AM.

Z	AM	A	B	C	D	E
17	35	0.015	0.192	0.049	0.065	0.255
17	37	0.011	0.140	0.036	0.048	0.187
19	39	0.005	0.09	0.026	0.024	0.116
21	45	1.34	19.6	6.54	3.22	25.3
23	51	3.02	39.5	13.7	4.65	54.5
25	55	2.51	29.7	11.9	2.88	41.8
27	59	6.38	71.6	30.7	5.84	108
29	63	2.79	30.1	13.8	2.14	49.1
29	65	3.30	35.6	16.3	2.53	58.1
31	69	3.30	34.6	17.0	2.19	61.7
33	75	2.36	23.9	12.7	1.40	46.8
35	79	6.55	65.8	37.5	3.52	142
35	81	7.79	78.4	44.7	4.18	169
37	85	2.98	29.4	18.2	1.49	70.1
37	87	14.9	148.0	91.2	7.38	353.0
39	89	0.081	0.799	0.537	0.038	2.1
41	93	81.7	793	584	36.5	2332
43	99	85.1	817	662	36.7	2674
45	103	0.060	0.567	0.509	0.025	2.0
47	107	0.115	1.08	1.08	0.047	4.4
47	109	0.155	1.45	1.45	0.064	5.9
49	115	134	1207	1381	54.3	5572
51	121	65.4	379	748	26.1	2279
51	123	35.1	203	401	14.0	1223
53	127	53.4	391	670	21.5	2398
55	133	46.2	117	653	18.2	1131
57	139	60.6	510	957	24.0	3883
59	141	159	1434	2801	63.1	11961

TABLE VI. Calculated ion temperatures at lasing conditions and fraction of gain coefficients due to the hyperfine splittings.

Z	AM	T_i (eV)	B	C	D
17	35	14.5	0.99	1.00	0.99
17	37	14.5	1.00	1.00	0.99
19	39	26	1.00	1.00	1.00
21	45	43	0.82	0.93	0.76
23	51	65	0.78	0.90	0.69
25	55	95	0.87	0.94	0.81
27	59	132	0.79	0.89	0.69
29	63	177	0.92	0.96	0.87
29	65	177	0.91	0.96	0.85
31	69	230	0.93	0.96	0.88
33	75	290	0.96	0.98	0.92
35	79	358	0.92	0.95	0.83
35	81	358	0.90	0.94	0.80
37	85	434	0.97	0.98	0.92
37	87	434	0.86	0.90	0.70
39	89	516	1.00	1.00	1.00
41	93	604	0.62	0.66	0.41
43	99	698	0.64	0.67	0.41
45	103	797	1.00	1.00	1.00
47	107	900	1.00	1.00	1.00
47	109	900	1.00	1.00	1.00
49	115	1010	0.64	0.59	0.40
51	121	1120	0.86	0.74	0.50
51	123	1120	0.92	0.84	0.63
53	127	1230	0.87	0.78	0.50
55	133	1340	0.96	0.80	0.69
57	139	1460	0.85	0.75	0.45
59	141	1570	0.69	0.52	0.44

Besides their role in the lasing systems, the observation of the hyperfine splittings are of interest. It is of interest to consider the direct observation of the splittings in nonlasing situations. In the case of the sodiumlike niobium 182-Å $3p_{1/2}$-to-$3s_{1/2}$ line, the four hyperfine components group themselves into two groups separated by 43 mÅ.

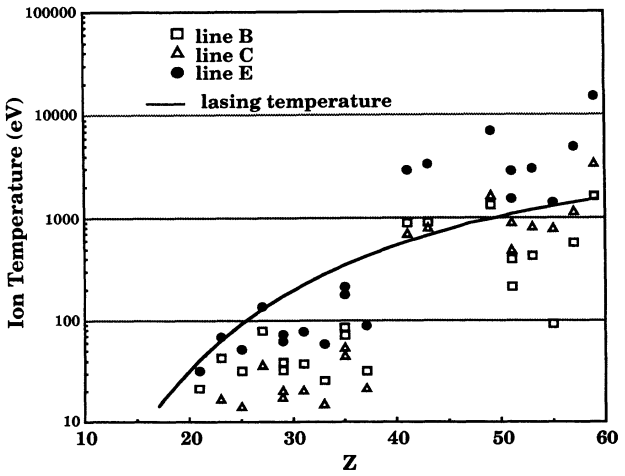

FIG. 5. Ion temperature for which the relative peak gain is at 70% due to hyperfine splittings for the three lines *B*, *C*, and *E* as a function of *Z*. The solid curve gives a model dependent set for the lasing ion temperatures.

TABLE VII. A_e values in meV for the $n=2$ F-like levels and the $n=3$ Na-like levels.

	Fluorinelike			Sodiumlike				
Z	$2p_{3/2}$	$2p_{1/2}$	$2s_{1/2}$	$3s_{1/2}$	$3p_{1/2}$	$3p_{3/2}$	$3d_{3/2}$	$3d_{5/2}$
17	0.023	0.119	0.427	0.058	0.015	0.003	0.001	0.000
19	0.035	0.180	0.633	0.099	0.027	0.005	0.002	0.001
21	0.050	0.260	0.899	0.155	0.044	0.008	0.003	0.001
23	0.069	0.361	1.23	0.229	0.065	0.013	0.005	0.002
25	0.092	0.487	1.64	0.322	0.094	0.018	0.007	0.003
27	0.120	0.641	2.15	0.439	0.129	0.024	0.011	0.005
29	0.153	0.827	2.75	0.581	0.173	0.032	0.014	0.006
31	0.192	1.048	3.46	0.753	0.226	0.042	0.019	0.008
33	0.237	1.31	4.30	0.958	0.290	0.053	0.025	0.011
35	0.289	1.61	5.28	1.20	0.366	0.066	0.032	0.013
37	0.347	1.97	6.41	1.49	0.455	0.081	0.039	0.017
39	0.414	2.38	7.72	1.82	0.559	0.098	0.048	0.020
41	0.488	2.85	9.22	2.20	0.681	0.117	0.059	0.025
43	0.571	3.39	10.9	2.64	0.821	0.139	0.070	0.029
45	0.663	4.01	12.9	3.15	0.982	0.164	0.083	0.035
47	0.764	4.71	15.1	3.73	1.17	0.191	0.098	0.041
49	0.876	5.51	17.7	4.39	1.38	0.221	0.114	0.047
51	0.999	6.42	20.5	5.14	1.62	0.254	0.132	0.055
53	1.13	7.44	23.8	6.00	1.89	0.291	0.152	0.063
55	1.28	8.60	27.4	6.96	2.20	0.331	0.174	0.072
57	1.44	9.91	31.6	8.06	2.56	0.375	0.198	0.081
59	1.61	11.4	36.2	9.30	2.96	0.423	0.224	0.092

Similarly, the 57-Å $2s_{1/2}$-to-$2p_{1/2}$ fluorinelike line has two groups split by 20 mÅ. Table VII presents the A_e values for the fluorine and sodiumlike ions and Fig. 6 presents the emission spectrum for the $2s_{1/2}$-to-$2p_{1/2}$ fluorinelike line for niobium shown with an ion temperature of 300 eV.

CONCLUSION

The hyperfine splittings certainly need to be taken into account for the nuclei with larger magnetic moments.

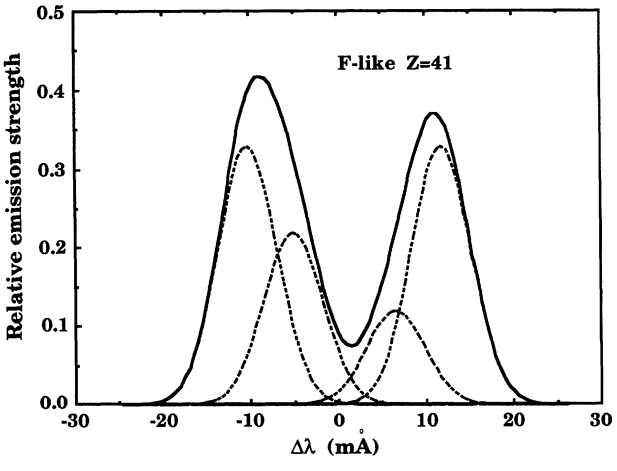

FIG. 6. Relative emission of the $2s_{1/2}$-to-$2p_{1/2}$ fluorinelike line in niobium as a function of wavelength due to the hyperfine splitting of niobium for an ion temperature of 300 eV. The dashed lines show the contributions due to each of the components.

Considering them gives a new dimension for understanding the laser emissions. For the Ne-like Nb x-ray laser the impact of the hyperfine splitting is dramatic. At present there is a puzzle in connection with the observations of lasing in the low-Z elements. Lasing on the $J=0\rightarrow 1$ line E has been observed for Ti ($Z=22$), Cr (24), Fe (26), and Ni (28). In experiments on Sc (21) and V (23) the line was so weak it was not detected. At an ion temperature of 50 eV for V, the expected drop in laser intensity by a factor of 50 as compared with Ti or Cr laser output should still have been detectable. The indication may be that the lasing is relying on lower ion temperatures than expected combined possibly with larger than expected loss mechanisms. The other odd-Z ions should also be affected in varying degrees. Qualitative comparisons between results with cobalt and nickel show much weaker emission from the cobalt [10], while lasing was not detected in manganese. Lasing is observed in copper [11,13]. This is presumably lessened to some extent by the hyperfine splittings. Systematic studies of the gains for the various ions and a better understanding of the plasma conditions are needed.

ACKNOWLEDGMENTS

The authors wish to thank Dr. Rosemary S. Walling for her assistance in the calculation of the plasma heating and Dr. Joseph Reader for helpful discussions. This work was performed under the auspices of the U.S. Department of Energy by the Lawrence Livermore National Laboratory under Contract No. W-7405-ENG-48.

[1] J. Nilsen J. A. Koch, J. H. Scofield, B. J. MacGowan, J. C. Moreno, and L. B. Da Silva, Phys. Rev. Lett. **70**, 3713 (1993).

[2] L. Pauli, Naturwiss **12**, 741 (1924); E. Fermi, Z. Phys. **60**, 320 (1930); Hargraeaves, Proc. R. Soc. London, Ser. A **124**, 568 (1929); **127**, 141 (1930); **127**, 407 (1930).

[3] See, *Hyperfine Interactions of Radioactive Nuclei,* edited by J. Christiansen (Springer-Verlag, Berlin, 1983).

[4] J. R. Henderson, P. Beiersdrofer, C. L. Bennett, S. Chantrenne, D. A. Knapp, R. E. Marrs, M. B. Schneider, K. L. Wong, G. A. Doschek, J. F. Seely, C. M. Brown, R. E. LaVilla, J. Dubau, and M. A. Levine, Phys. Rev. Lett. **65**, 705 (1990).

[5] B. B. Birkett, J.-P. Briand, P. Charles, D. D. Dietrich, K. Finlayson, P. Indelicato, D. Liesin, R. Marrus, and A. Simionovici, Phys. Rev. A **47**, R2454 (1993).

[6] J. O. Ekberg and J. Reader, J. Opt. Soc. Am. B (to be published).

[7] Thomas U. Kühl (private communication).

[8] T. Boehly, M. Russotto, R. S. Craxton, R. Epstein, B. Yaakobi, L. B. Da Silva, J. Nilsen, E. A. Chandler, D. J. Fields, B. J. MacGowan, D. L. Matthews, J. H. Scofield, and G. Shimkaveg, Phys. Rev. A **42**, 6962 (1990).

[9] J. Nilsen, B. J. MacGowan, L. B. Da Silva, and J. C. Moreno, Phys. Rev. A **48**, 4682 (1993).

[10] J. Nilsen, B. J. MacGowan, L. B. Da Silva, J. C. Moreno, J. A. Koch, and J. H. Scofield, in *Ultrashort Wavelength Lasers II,* edited by S. Sackewer, SPIE Proc. Vol. 2012 (SPIE, Bellingham, WA, 1994).

[11] J. Nilsen, J. C. Moreno, B. J. MacGowan, and J. A. Koch, Appl. Phys. B **57**, 309 (1993).

[12] J. Nilsen, J. L. Porter, B. J. MacGowan, L. B. Da Silva, and J. C. Moreno, J. Phys. B **26**, L243 (1993).

[13] R. C. Elton, *X-rays Lasers* (Academic, San Diego, 1990), pp. 99–198.

[14] B. J. MacGowan, M. D. Rosen, M. J. Eckart, P. L. Hagelstein, D. L. Matthews, D. J. Nilson, T. W. Pillips, J. H. Scofield, G. Shimkaveg, J. E. Trebes, R. S. Walling, B. L. Whitten, and J. G. Woodworth, J. Appl. Phys. **61**, 5243 (1987).

[15] D. J. Fields, R. S. Walling, G. M. Shimkaveg, B. J. MacGowan, L. B. Da Silva, J. H. Scofield, A. L. Osterheld, T. W. Phillips, M. D. Rosen, D. L. Matthews, W. H. Goldstein, and R. E. Stewart, Phys. Rev. A **46**, 1606 (1992).

[16] M. J. Eckart, J. H. Scofield, and A. U. Hazi, J. Phys. (Paris) Colloq. **49**, C1 (1988).

[17] G. D. Enright, D. M. Villeneuve, J. Dunn, H. A. Baldis, J. C. Kieffer, H. Pépin, M. Chaker, and P. R. Herman, J. Opt. Soc. Am. B **8**, 2047 (1991).

[18] C. Schwartz, Phys. Rev. **97**, 380 (1955).

[19] I. I. Sobel'man, *Introduction to the Theory of Atomic Spectra* (Pergamon, Oxford, 1972), p. 204 ff.

[20] K. T. Cheng and W. J. Childs, Phys. Rev. A **31**, 2775 (1985).

[21] I. P. Grant, B. J. McKenzie, P. H. Norrington, D. F. Mayers, and N. C. Pyper, Comput. Phys. Commun. **21**, 207 (1980); B. J. McKenzie, I. P. Grant, and P. H. Norrington, *ibid.* **21**, 233 (1980); K. G. Dayall, I. P. Grant, C. T. Johnson, F. A. Paripia, and E. P. Plummer, *ibid.* **55**, 425 (1989); F. A. Parpia, I. P. Grant, and C. Froese Fischer (private communication).

[22] G. Racah, Nuovo Cimento **8**, 178 (1931), Z. Phys. **71**, 431 (1931); H. B. G. Casimir, *On the Interaction between Atomic Nuclei and Electrons* (Freeman, San Francisco, 1963).

[23] A. Bohr and V. F. Weisskopf, Phys. Rev. **77**, 94 (1950).

[24] *Table of Isotopes,* edited by C. M. Lederer and V. S. Shirley (Wiley, New York, 1978).

[25] M. D. Rosen, R. A. London, and P. L. Hagelstein, Phys. Fluids **31**, 666 (1988).

[26] B. L. Whitten, R. A. London, and R. S. Walling, J. Opt. Soc. Am. B **12**, 2537 (1988).

[27] G. B. Zimmerman and R. M. More, Comments Plasma Phys. and Controlled Fusion **2**, 51 (1975).

[28] M. D. Rosen, P. L. Hagelstein, D. L. Matthews, E. M. Campbell, A. U. Hazi, B. L. Whitten, B. MacGowan, R. E. Turner, and R. W. Lee, Phys. Rev. Lett. **54**, 106 (1985).

[29] J. A. Koch, B. J. MacGowan, L. D. Da Silva, D. L. Matthews, J. H. Underwood, P. J. Batson, and S. Mrowka, Phys. Rev. Lett. **68**, 3291 (1992).